Numerical analysis of solute segregation at Σ5 (310)/[001] symmetric tilt grain boundaries in Y_2O_3-doped ZrO_2

Takashi Oyama, Masato Yoshiya,* and Hideaki Matsubara
Japan Fine Ceramics Center, 2-4-1, Mutsuno, Atsuta-ku, Nagoya 456-8587, Japan

Katsuyuki Matsunaga
Institute of Engineering Innovation, The University of Tokyo, 2-11-16, Yayoi, Bunkyo-ku, Tokyo 113-8656, Japan
(Received 3 December 2004; published 15 June 2005)

Atomistic mechanisms that determine atomic coordination and local concentration of dopants at Σ5 (310)/[001] symmetric tilt grain boundaries in Y_2O_3-doped ZrO_2 are analyzed using atomistic simulation techniques. Segregation mechanisms are found to be different from those in metals or metalloids, with local strain relief controlled by short-range interactions, which act as the driving force for segregation, while long-range Coulombic interactions between the grain boundary region and the dopants resist segregation. It is found that Y^{3+} ions segregate to a region within around 0.6 nm either side of the grain boundary plane. The equilibrium local concentration of dopants in the vicinity of the grain boundary, which is determined by the balance between repulsive forces between dopants and the grain boundary and attractive forces associated with local strain relief, is calculated to be 16.7 mol % for 10.3 mol % Y_2O_3-doped ZrO_2. Cosegregation of an O^{2-} vacancy is necessary to accommodate a Y^{3+} ion at the Σ5 grain boundary; O^{2-} vacancies play important roles in reducing repulsion between dopants and the grain boundary and relieving local strain further. These conclusions are supported by Monte Carlo simulations using an unrestricted model. Segregation-induced modifications to the grain boundary structure observed in the simulations are used to interpret experimental HREM and *Z*-contrast images.

DOI: 10.1103/PhysRevB.71.224105 PACS number(s): 68.35.Dv, 61.72.Mm, 81.05.Je, 02.70.−c

I. INTRODUCTION

Controlling grain boundary (GB) structures and chemistry is an important issue in the development of advanced materials such as oxide ceramics, since their macroscopic properties are often governed by their GB properties. When impurities and dopants are present, they often segregate at GBs, which strongly affects the GB chemistry. Therefore, it is important to understand segregation behavior at GBs in the materials. So far, a number of theoretical models for GB segregation, such as the Langmuir-McLean and BET models,[1–3] have been proposed, but they are based on combinations of macroscopic thermodynamics and statistical mechanics. In this case, in order to predict segregation behavior, it is necessary to quantitatively determine the interactions between a GB and a single dopant atom, and between different dopant atoms. In addition, the space charge theory[3–6] is commonly used to explain segregation of intrinsic defects, impurities, and dopants at GBs in oxide ceramics. Since point defects in oxide materials have effective charges, preferential segregation of a particular charged defect species results in formation of a space charge at the GB, where the driving force for segregation is basically the difference in formation energies of possible defect species. Although this theory can provide quantitative understanding of segregation behavior, the atomic-scale GB structures are not taken into account in this theory. It is known that GB structures depend on GB characters such as grain misorientation and crystallographic GB planes, which would affect segregation. Thus, it is desirable to examine dopant segregation in terms of the atomic structure of GBs.

In this study, atomistic mechanisms of dopant segregation in Y_2O_3-doped cubic ZrO_2 [yttria-stabilized zirconia (YSZ)] are investigated. This is an example of a material in which foreign ions and defects are present both at GBs and in the grain interiors. Aliovalent dopant containing ZrO_2, such as YSZ, is widely used as an electrolyte in solid oxide fuel cells[7,8] and oxygen gas sensors.[9] Its oxide ion conductivity at elevated temperatures is dramatically increased by addition of M_2O_3 or MO, where M is a divalent or trivalent cation, owing to formation of O^{2-} vacancies to maintain charge neutrality.[10,11] It is well known that GBs in polycrystalline ZrO_2 are a source of resistance to oxide ion conduction.[12–15] Fisher *et al.* pointed out that the resistance is caused by the structural discontinuity at GBs and is enhanced by GB segregation of dopant ions.[16] On the other hand, with suitable doping, ZrO_2 can be prepared with grains finer than 1 μm in diameter and made to exhibit superplastic deformation at elevated temperatures.[17–19] This superplasticity phenomenon is due to GB sliding.[20] It is believed that GB sliding is facilitated by dopant ions segregated at GBs since they relieve stress effectively upon sliding.[21–23] GB segregation therefore needs to be controlled to optimize both the electrical and mechanical properties of polycrystalline ZrO_2.

In recent years, structures of various GBs in ZrO_2 have been investigated using transmission electron microscopy (TEM) and scanning transmission electron microscopy (STEM). These studies revealed aspects such as the relationship between atomic structure of a GB and its properties; the relationship between interfacial energy and misorientation between two grains has also been examined quantitatively in these studies.[24–28] Local chemistry at GBs has also been ana-

lyzed using spectroscopic methods such as x-ray energy dispersive spectroscopy (EDS) and electron energy loss spectroscopy (EELS) in combination with TEM or STEM.[26–31] Of various zirconia synthesized, YSZ is the most studied with respect to structures and compositions of its GBs.[27–31] These investigations have shown that no interstitial cations or amorphous layers are found at GBs (in high-purity, silica-free materials) and Y^{3+} ions segregate within a few nanometers of a GB plane. However, while two-dimensional cation coordination at GBs has been determined with high accuracy using HREM and *Z*-contrast images, the spatial distribution of Y^{3+} ions and O^{2-} vacancies across GBs has not been clarified on the atomic level, because at present EDS and EELS techniques do not have enough sensitivity or spatial resolution to identify individual Y^{3+} ions or vacancies on Zr^{4+} or O^{2-} sites, respectively.

Numerical analyses using atomistic simulations have led to further understanding of GB segregation.[32–36] In the case of YSZ, simulations allow the spatial distribution of Y^{3+} ions to be examined on the atomic level. Sawaguchi *et al.*, based on results of Monte Carlo simulations, reported that Y^{3+} ions occupy Zr^{4+} sites within several atomic layers from GB planes.[37] Lei *et al.* also obtained a similar result using a distance-valence least-squares method.[30] These phenomenological simulations demonstrated that segregation is energetically favorable in YSZ. However, detailed mechanisms of dopant segregation have not yet been reported.

A few interesting observations have been made with respect to the driving force for segregation in YSZ. Shibata *et al.* pointed out that the segregation at $\Sigma 3$ $(111)/[110]$ symmetric tilt GBs is closely related to the change in coordination number of Zr^{4+} sites at the GB core.[27] Mao *et al.* pointed out that Y^{3+} ions preferentially occupy Zr^{4+} sites at the $\Sigma 5$ $(310)/[001]$ symmetric tilt GBs because of the greater free volume at such sites.[38] These observations suggest that the irregular coordination environment of Zr^{4+} sites in the vicinity of a particular GB core is one of the driving forces for segregation. However, Zr^{4+} sites with nontypical or irregular coordination environments (relative to the bulk) are too few to account for the local concentration of Y^{3+} ions at GBs observed experimentally.[27,29] Furthermore, the role of O^{2-} vacancies in the segregation process has not been addressed in these discussions. Lack of understanding of these issues is an impediment to the control of grain boundary composition and, in turn, control of the electrical and mechanical properties of polycrystalline ZrO_2. Deeper understanding is therefore needed to improve the properties and performance of these materials.

In this study, mechanisms of GB segregation of Y^{3+} ions in YSZ have been investigated using atomistic simulation techniques. A $\Sigma 5$ $(310)/[001]$ symmetric tilt GB was chosen as a model boundary since the local concentration of Y^{3+} ions and cation coordination at this GB have been measured experimentally.[29] The driving force for the segregation and spatial distribution of Y^{3+} ions across the GB on the atomic level are discussed in Sec. III A. Mechanisms that determine the local concentration of Y^{3+} ions in the vicinity of the GB are addressed in Sec. III B. In Sec. III C, these results are compared with an unrestricted model simulating site interchange by the Monte Carlo technique. Segregation-induced modification of the GB structure is analyzed in Sec. III D. Conclusions are given in Sec. IV.

II. COMPUTATIONAL PROCEDURE

A. Lattice statics calculation

When Y_2O_3 is added to ZrO_2, Y^{3+} ions substitute for Zr^{4+} ions, with one O^{2-} vacancy formed for every two Y^{3+} ions added:

$$Y_2O_3 \rightarrow 2Y'_{Zr} + V_O^{\bullet\bullet} + 3O_O^{\times}. \tag{1}$$

In order to investigate the mechanisms controlling the spatial distribution of Y^{3+} ions and O^{2-} vacancies across the GB and local concentration of Y^{3+} ions in the vicinity of the GB, energies of a YSZ supercell containing the GB were calculated as a function of the spatial distribution and local concentration using the energy minimization method known as the lattice statics method. Using this method, for a given set of potential parameters, both an optimized structure and its lattice energy under static condition are obtained. This method can also handle a relatively large number of ions within a reasonable time compared with computationally expensive first-principles methods, so that a large number of different segregation configurations can be studied in a systematic way.

The lattice energy of an ionic compound E_{tot} is given as

$$E_{\text{tot}} = E^C + E^{\text{SR}} = \frac{1}{2}\sum_i \sum_{j\neq i} (\phi_{ij}^C + \phi_{ij}^{\text{SR}}), \tag{2}$$

where E^C is the long-range Coulombic energy due to interactions between charged species and E^{SR} is the short-range interaction energy resulting from electron cloud overlap and van der Waals dispersion forces. Energies are given by a sum over all ionic pairs, with the Ewald method[39] used for the Coulombic part of the summation. The components in round brackets in Eq. (2), namely, ϕ_{ij}^C and ϕ_{ij}^{SR}, are pairwise potentials of the Coulombic and the short-range interactions, respectively. A simple Buckingham type potential function was employed for ϕ_{ij}^{SR}, which is given by

$$\phi_{ij}^{\text{SR}}(r_{ij}) = A_{ij}\exp\left(\frac{-r_{ij}}{\rho_{ij}}\right) - \frac{C_{ij}}{r_{ij}^6}, \tag{3}$$

where A_{ij}, ρ_{ij}, and C_{ij} are potential parameters for a pair of ions i and j and r_{ij} is the distance between them. The parameters developed by Minervini *et al.*, which are summarized in Table I,[40,41] were used in this study since they successfully reproduce the most stable configuration of an O^{2-} vacancy with respect to a Y^{3+} ion in bulk ZrO_2 observed experimentally.[42] One limitation of our simple two-body potential model is that it fails to reproduce the low-temperature, monoclinic structure of pure ZrO_2; a cubic structure is obtained instead. This is not a serious limitation because at yttria concentrations above 8 mol %, the cubic structure can be stabilized at low temperatures. At GBs to which Y^{3+} ions have segregated, the Y^{3+} concentration will be higher than in the bulk, so it is reasonable to assume a cubic structure for all our simulations. Interatomic interactions are truncated at

TABLE I. Short-range potential parameters for the Buckingham-type pairwise potential function used in this study.

Ion pair	A (eV)	ρ (10^{-2} nm)	C (10^{-6} eV nm^6)
$Zr^{4+}-O^{2-}$	1502.11[a]	3.4770[a]	5.10[a]
$Y^{3+}-O^{2-}$	1766.40[b]	3.3849[b]	19.43[b]
$O^{2-}-O^{2-}$	9547.96[b]	2.1920[b]	32.00[b]

[a]Ref. 40.
[b]Ref. 41.

$r=2$ nm. All lattice statics calculations were carried out at constant pressure using the GULP code.[43]

The supercell for the GB model contained two identical Σ5 symmetric GBs after applying three-dimensional periodic boundary conditions. As shown in Fig. 1, the supercell was eight Σ5 coincidence site lattice (CSL) unit cell lengths (6.424 nm) perpendicular to the GB plane, and one Σ5 CSL unit cell length (0.803 nm) and two fluorite unit cell lengths (1.016 nm) along the two axes parallel to the GB plane. The supercell consisted of 156 Zr^{4+} and 312 O^{2-} ions in the case of pure ZrO_2. As a result, the GBs were separated by four Σ5 CSL unit lengths (3.212 nm) to ensure no interaction between the GBs. The initial ion configuration in the vicinity of the GBs generated by CSL theory[44] was modified slightly to minimize interfacial energy; some of the ions positioned too close together were removed or shifted. The relaxed GB structure obtained in this way, shown in Fig. 2, agrees well with that reported by Fisher *et al.*[16] and Mao *et al.*[38] For bulk model calculations, a supercell in which the fluorite unit cell was multiplied four times in each of the three directions was used.

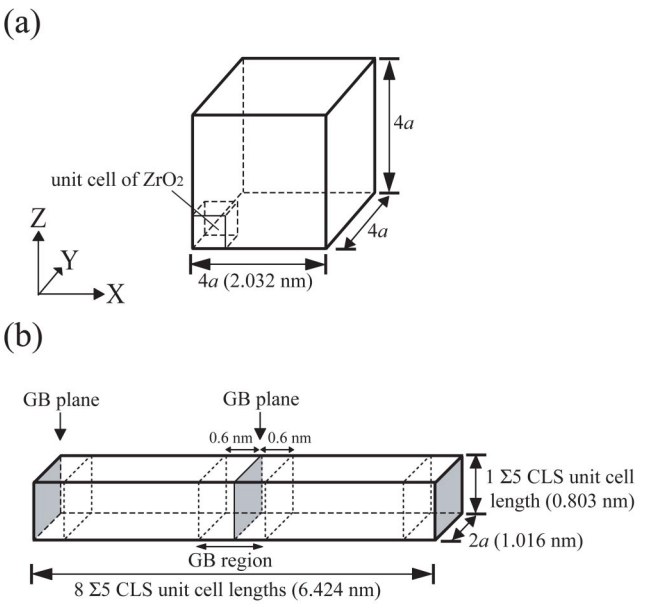

FIG. 1. Schematic diagrams of supercells: (a) the bulk model representing grain interior and (b) the Σ5 GB model, where a is the lattice constant for pure cubic ZrO_2. The GB region, defined as a 1.2-nm-thick slice with the interface plane at its center, is shown in the latter.

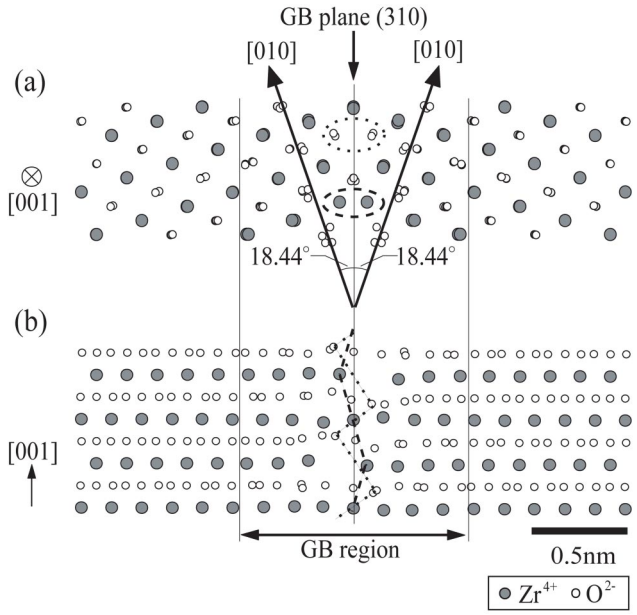

FIG. 2. Atomic configuration of a Σ5 (310)/[001] symmetrical tilt grain boundary for pure ZrO_2 projected onto two planes: (a) parallel to [001], and (b) perpendicular to [001]. It is noted that, to reduce repulsive forces between ions of like sign, columns of Zr^{4+} and O^{2-} ions in the vicinity of the GB plane indicated by broken and dotted circles, respectively, are half filled, and the Zr^{4+} and O^{2-} ions are aligned in a zigzag manner indicated by broken and dotted lines, respectively.

B. Monte Carlo simulation

In order to obtain configurations of Y^{3+} ions and O^{2-} vacancies in the bulk and around the Σ5 GB, Monte Carlo simulations involving interchange of dopant and vacancy sites were carried out. During these simulations, positions of Y^{3+} ions and O^{2-} vacancies were changed according to a Monte Carlo algorithm, and the lattice energies of supercells with various defect configurations were calculated by an energy minimization technique similar to that used for the lattice statics calculations. Through a combination of these two techniques, an optimum configuration was obtained.

In the initial configuration, Y^{3+} ions were randomly substituted for Zr^{4+} ions and the corresponding number of O^{2-} ions removed randomly to maintain charge neutrality. At each step of the Monte Carlo simulation, a randomly selected Y^{3+} ion or O^{2-} vacancy was interchanged with a Zr^{4+} or O^{2-} ion, respectively, that had been chosen randomly from their nearest neighbor sites. This was followed by a lattice statics calculation for the new configuration. From difference in lattice energy upon exchanging defect sites, it was judged whether the interchanged configuration was acceptable or not. Using the Metropolis method,[45] the acceptance ratio of a trial R_a was given by

$$R_a = \begin{cases} 1 & (\Delta E_{\text{tot}} < 0), \\ \exp\left(-\dfrac{\Delta E_{\text{tot}}}{k_B T}\right) & (\Delta E_{\text{tot}} \geqslant 0), \end{cases} \tag{4}$$

where k_B is Boltzmann's constant and T is temperature, which was set to 300 K in this study to permit slight thermal

fluctuation. The lattice energy difference ΔE_{tot} was calculated according to

$$\Delta E_{tot} = E_{after} - E_{before}, \tag{5}$$

where E_{after} and E_{before} are the lattice energies of the configurations before and after exchanging defect sites, respectively. When ΔE_{tot} was negative, the exchange was automatically accepted. When it was positive, the trial was accepted if R_a was larger than a random number between 0 and 1. Optimization of a configuration was repeated until the lattice energy of the supercell converged to within the fluctuations at 300 K with increasing Monte Carlo steps. Interatomic interactions were truncated at $r=0.8$ nm in the energy minimization part of the Monte Carlo simulations to reduce computational time.

III. RESULTS AND DISCUSSION

A. Driving force for GB segregation

In this section, the energetics of GB segregation of Y'_{Zr} and $V^{\bullet\bullet}_O$ species are discussed to clarify the driving force behind the GB segregation process. In order to simplify the analysis, two segregation models were considered. The first model is the Y'_{Zr} model, in which only one Y^{3+} ion was introduced at a Zr^{4+} site in a pure $\Sigma 5$ GB ZrO_2 supercell. In the second which we call the $(Y'_{Zr}:V^{\bullet\bullet}_O)^{\bullet}$ model, a pair of Y'_{Zr} and $V^{\bullet\bullet}_O$ species was placed near the GB. In the latter model, it was assumed that the O^{2-} vacancy was located at a next nearest neighbor site to the Y^{3+} ion. This is because previous atomistic simulation studies have shown that such a $Y'_{Zr}-V^{\bullet\bullet}_O$ configuration is energetically favorable.[42]

The segregation energy of Y'_{Zr} or a $Y'_{Zr}-V^{\bullet\bullet}_O$ pair at the GB $E_{seg}(r)$ was obtained from the lattice energies of the supercells $E_{tot}(r)$ as follows:

$$E_{seg}(r) = E_{tot}(r) - E_{tot}(\infty), \tag{6}$$

where r is the distance of a defect from the GB plane. In order to calculate $E_{tot}(\infty)$, which corresponds to when a Y'_{Zr} or $Y'_{Zr}-V^{\bullet\bullet}_O$ pair is infinitely separated from the GB plane, a defect was introduced at $r=1.62$ nm (at the center of one of the crystal slabs in the GB supercell) and its lattice energy is calculated. It is noted here that, in the presence of a single Y'_{Zr} ion or $Y'_{Zr}-V^{\bullet\bullet}_O$ pair, the charge neutrality of the GB supercell is not maintained. Therefore, $E_{tot}(r)$ values were calculated with a uniform neutralizing background charge; this contribution to the energy is cancelled in Eq. (6). In addition, for the $Y'_{Zr}-V^{\bullet\bullet}_O$ pair, three kinds of $V^{\bullet\bullet}_O$ positions with respect to Y'_{Zr} were considered, and their lattice energies were averaged to obtain $E_{tot}(r)$.

Figure 3 shows variations of $E_{seg}(r)$ per defect as a function of distance r. In the Y'_{Zr} model, the segregation energy $E_Y(r)$ increased with decreasing $Y'_{Zr}-$GB distances, and exhibited positive values within ca. 0.6 nm from the GB plane. In contrast, $E_{seg}(r)$ for the $(Y'_{Zr}:V^{\bullet\bullet}_O)^{\bullet}$ model $E_{YV}(r)$ decreased as the pair moved closer to the GB, which results in negative values for $r \leqslant 0.6$ nm. It can be said, therefore, that an isolated Y'_{Zr} receives an energy penalty by segregation to the GB, but tends to segregate when it is accompanied by an

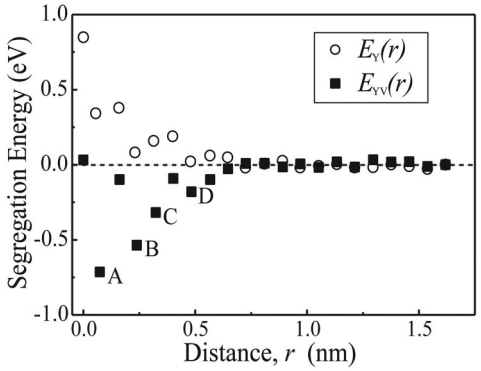

FIG. 3. Segregation energies for Y'_{Zr} and $(Y'_{Zr}:V^{\bullet\bullet}_O)^{\bullet}$ models as a function of distance from the GB plane. Open circles and filled squares are for the Y'_{Zr} and $(Y'_{Zr}:V^{\bullet\bullet}_O)^{\bullet}$ models, respectively. Labels A-D indicate the Zr^{4+} sites with irregular coordination environments illustrated in Fig. 8.

O^{2-} vacancy. According to the analysis by Guo *et al.*,[6] Y^{3+} ions segregate at YSZ GBs, whereas the concentration of O^{2-} vacancies decreases due to the space charge effect, which is quite different from the present results. Therefore, it can be expected that Y^{3+} segregation behavior cannot be simply explained by the space charge effect, but is also closely related to segregation of O^{2-} vacancies. The cosegregation of an Y^{3+} ion and O^{2-} vacancy takes place within a region 0.6 nm either side of the GB plane, which is much smaller than that suggested by experiment. It is noted that, even for the pair segregation, there exist a few sites where occupation by Y^{3+} is energetically more expensive. This is known as site selectivity of segregation.[46,47]

Preliminary analysis of the segregation energies showed that they were not a simple function of the oxygen coordination number of Y^{3+} ions or interatomic distance between Y^{3+} ions and its O^{2-} neighbors. A combination of these two factors was also found to be unsuccessful in explaining quantitatively the segregation phenomenon and its associated energies. This is because the distortion to the lattice and vacancy distribution caused by the presence of the dopant affects not only the immediate environment of the dopant (its nearest neighbors), but the cations and anions several coordination shells beyond as well. In order to analyze the segregation energies in more detail, the segregation energies were divided into their Coulombic components $E^C_Y(r)$ and $E^C_{YV}(r)$ and short-range components $E^{SR}_Y(r)$ and $E^{SR}_{YV}(r)$ for the Y'_{Zr} and $(Y'_{Zr}:V^{\bullet\bullet}_O)^{\bullet}$ models, respectively. Such a strategy allows the influence of changes in coordination and structure beyond the nearest neighbors of a dopant to be taken into account. Combining Eqs. (2) and (6), the segregation energy can therefore be expressed

$$E_{seg}(r) = E^C_{seg}(r) + E^{SR}_{seg}(r). \tag{7}$$

Figures 4(a) and 4(b) show plots of these components as a function of distance r. Both $E^C_{YV}(r)$ and $E^{SR}_{YV}(r)$ were around 0 eV for $r > 0.6$ nm. $E^C_{YV}(r)$ increased with decreasing r below $r=0.6$ nm. This is a consequence of the increasing Coulombic repulsion between the GB and the charged dopant

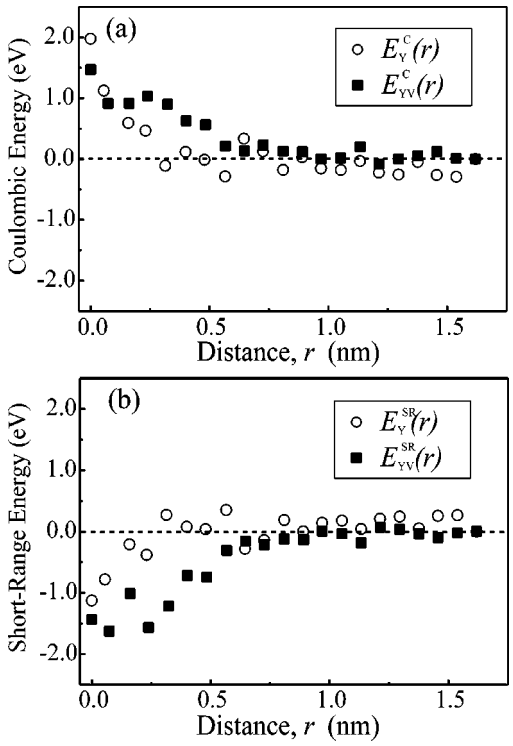

FIG. 4. Components of segregation energies for Y'_{Zr} and $(Y'_{Zr}:V_O^{\bullet\bullet})^{\bullet}$ models as a function of distance from the GB plane: (a) Coulombic components and (b) short-range components. Open circles and filled squares are for the Y'_{Zr} and $(Y'_{Zr}:V_O^{\bullet\bullet})^{\bullet}$ models, respectively.

species as the dopant approaches the GB. In contrast, $E_{YV}^{SR}(r)$ decreased with decreasing r for $r \leqslant 0.6$ nm. Since the effective volumes of a Y^{3+} ion and O^{2-} vacancy are different from those of the respective Zr^{4+} ion and O^{2-} ion they replace, a local lattice strain exists around them. The local strain is mainly manifested in the short-range term. The decrease in the short-range components shown in Fig. 4(b) therefore indicates that the local strain is relieved as the $Y'_{Zr}-V_O^{\bullet\bullet}$ pair approaches the GB. The magnitude of the decrease in $E_{YV}^{SR}(r)$ is larger than the increase in $E_{YV}^{C}(r)$. Hence, the sum of these, $E_{YV}(r)$, decreased as r decreased for $r \leqslant 0.6$ nm, stabilizing the pair segregation. In contrast, while $E_Y^C(r)$ was around 0 eV for $r > 0.6$ nm, it increased rapidly as r decreased below $r \leqslant 0.6$ nm. $E_Y^{SR}(r)$, however, did not decrease as much as that for the pair segregation as the defect approached the GB plane. This may be explained as follows. $V_O^{\bullet\bullet}$ has a positive effective charge, which counteracts the negative effective charge of Y'_{Zr}, thereby reducing the net repulsion between the GB and dopants. In addition, O^{2-} vacancies are known to relieve the local strain imposed on neighboring Zr^{4+} ions by Y^{3+} substitution; Zr^{4+} ions prefer seven-fold coordination, while Y^{3+} prefers eight-fold coordination.[48] Since Y'_{Zr} and $V_O^{\bullet\bullet}$ defects produce elastic strain fields around them that are opposite, the excess strain energies of the defects could be reduced by pair formation. Since there is no vacancy in the Y'_{Zr} model to relieve the lattice strain caused by Y'_{Zr}, $E_Y^{SR}(r)$ is greater than $E_{YV}^{SR}(r)$, as shown in Fig. 4(b). As a result, $E_Y(r)$ is positive in the vicinity of the GB, indicating that segregation of Y^{3+} ions without O^{2-} vacancies is energetically unfavorable.

B. Local concentration of Y^{3+} ions at a GB

According to the Gibbs adsorption isotherm, the local concentration of solute at an interface depends on the chemical potential of a solute and the decrease in lattice strain when the interface and bulk are in a state of equilibrium.[49] However, factors that might influence the resulting properties such as local bond geometry and the spatial distribution of solute ions are not considered explicitly in Gibbs' theory since it is a macroscopic theory;[3] structural discontinuities, lattice distortion, and various kinds of defects at the interface are not taken into account, while segregants are assumed to lie on the GB plane. In fact, it is known that in the vicinity of the GB, coordination environments differ from those in bulk,[27,28] and segregants settle within several atomic layers from the GB plane[30,37] rather than on the GB plane itself. Therefore, chemical potentials need to be calculated taking into account these variations in atomic structure in order to reliably predict segregation concentrations and their effect on materials properties. Our aim in this section is to describe the atomistic mechanisms that determine the local concentration of Y^{3+} ions at the GB by calculating chemical potentials using models containing various concentrations of Y^{3+}.

Chemical potentials of Y^{3+} ions were calculated as a function of local concentration of Y^{3+} in the GB and bulk regions. The chemical potential μ is defined in this study as

$$\mu(n_Y) = \frac{dE_{tot}(n_Y)}{dn_Y}, \tag{8}$$

where E_{tot} is the lattice energy and n_Y is the number of Y^{3+} ions in each region. It is numerically calculated by

$$\mu(n_Y) = \frac{1}{2}\left[\frac{E_{tot}(n_{Y+4}) - E_{tot}(n_Y)}{4} + \frac{E_{tot}(n_Y) - E_{tot}(n_{Y-4})}{4}\right]$$
$$= \frac{1}{8}[E_{tot}(n_{Y+4}) - E_{tot}(n_{Y-4})]. \tag{9}$$

In this study, the entropy term was neglected, since we assume the segregation is mainly dependent on the enthalpy term. The chemical potential is therefore a measure of the variation in lattice energy when a $YO_{1.5}$ cluster replaces a ZrO_2 cluster. Chemical potentials in the GB region μ_{GB} and bulk region μ_{bulk} were calculated using the GB model and the bulk model, respectively, described in the previous section. In the GB model, Y'_{Zr} and $V_O^{\bullet\bullet}$ were confined to within 0.6 nm of the GB plane in accordance with the results of Sec. III A. Configurations of Y'_{Zr} and $V_O^{\bullet\bullet}$ were varied until the cell with the energy of its local minimum was found using the Monte Carlo technique. In the case of the GB model, site interchange was permitted only in the GB region; outside the GB region no Y^{3+} ion was present. To reduce the effect of errors associated with the small size of the supercell used in this study, μ_{GB} and μ_{bulk} were averaged over 8 and 30 calculations, respectively, of slightly different Y'_{Zr} and $V_O^{\bullet\bullet}$ configurations as obtained from Monte Carlo optimization after convergence. The local concentration of Y^{3+} ions in the

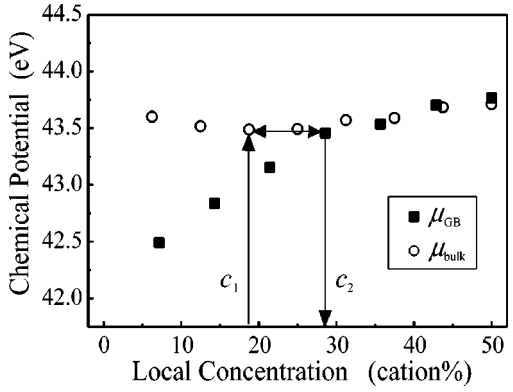

FIG. 5. Local concentration dependence of chemical potentials in the GB and bulk regions. Open circles and filled squares are for the bulk and GB regions, respectively. Arrows indicate equilibration of Y^{3+} ions between the GB and grain interior in the case of 10.3 mol % Y_2O_3-doped ZrO_2.

GB region c_{GB} was calculated as the ratio of the number of Y^{3+} ions in the 1.2-nm-wide GB region to the number of cations Zr^{4+} and Y^{3+} in the GB region. Outside the GB region, neither Y^{3+} ion nor O^{2-} vacancies were substituted in the GB model. The local concentration of Y^{3+} ions in the bulk region c_{bulk} was simply taken as the ratio of the total number of Y^{3+} ions to that of the total number of cations in the bulk model. Both of these ratios are expressed as cation concentrations (cation %).

Figure 5 shows chemical potentials in the GB and bulk regions as a function of local dopant concentration in each region. μ_{bulk} showed a slight change with increasing c_{bulk}. In contrast, μ_{GB} started at a smaller value and increased with increasing c_{GB}. Above 28.6%, both chemical potentials were similar in value.

As mentioned above, the amount of dopants at the GB is determined by considering the equilibrium between the dopants, interface and bulk structures. When the macroscopic concentration of dopants is equal to c_1,

$$c_{bulk} \cong c_1 \tag{10}$$

since the volume fraction of the GB region is negligibly small. In this case, μ_{GB} and μ_{bulk} satisfy

$$\mu_{GB}(c_2) = \mu_{bulk}(c_1). \tag{11}$$

This relation yields the local concentration of Y^{3+} ions in the GB region c_2. For example, for 10.3 mol % = 18.8 cation % Y_2O_3-doped ZrO_2, μ_{bulk} was 43.5 eV. μ_{GB} is equal to μ_{bulk} when c_2 reaches 28.6 cation %. Thus, Y^{3+} ions are enriched to 16.7 mol % (28.6 cation %) in the GB region in 10.3 mol % Y_2O_3-doped ZrO_2. The width of the GB region determined by experiment has been reported to be larger than calculated one due to limitations in spatial resolution. This is important, since the value of the local concentration changes with the definition of the GB width. If the GB region is extended to that reported from experiment, the value obtained is in good agreement with experiment.[29]

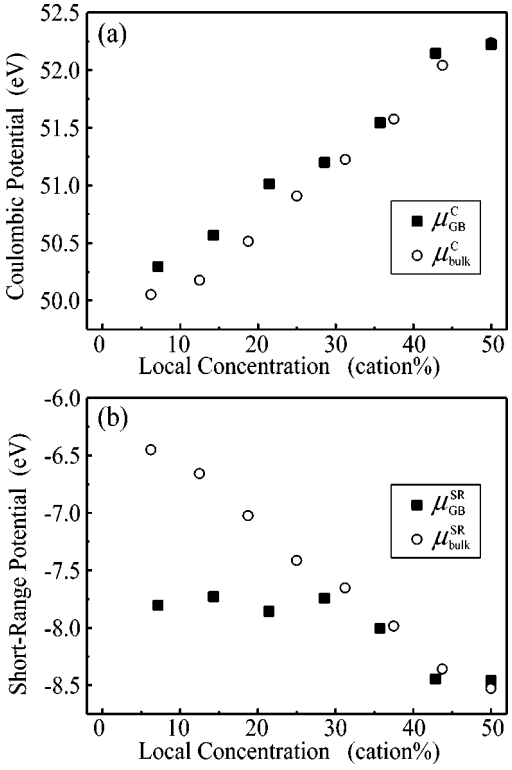

FIG. 6. Components of chemical potentials in the GB and bulk regions as a function of local concentration: (a) Coulombic component and (b) short-range component. Open circles and filled squares are for the bulk and GB regions, respectively.

The chemical potential for each region is given by a sum of the Coulombic and short-range components. As shown in Sec. III A, partitioning energy into these components provides detailed physical insights into the segregation. In the same way, the chemical potentials can also be separated into the Coulombic components μ^C and the short-range components μ^{SR} according to Eqs. (2) and (8). These components satisfy

$$\mu = \mu^C + \mu^{SR} \tag{12}$$

since

$$\frac{dE_{tot}}{dn_Y} = \frac{dE^C}{dn_Y} + \frac{dE^{SR}}{dn_Y}. \tag{13}$$

Figure 6(a) shows the Coulombic components of the chemical potentials in the GB region μ^C_{GB} and bulk region μ^C_{bulk} as a function of local concentration. Both μ^C_{GB} and μ^C_{bulk} had similar values for all local concentrations and they increased monotonically with increasing local concentration. Since the average distance between $YO_{1.5}$ clusters decreases with increasing concentration, Coulombic repulsion between the clusters increases as the distance is reduced unless they are perfectly ordered. Consequently, both Coulombic components increased with increasing local concentration.

Figure 6(b) shows the short-range components of the chemical potentials in the GB region μ^{SR}_{GB} and bulk region μ^{SR}_{bulk} as a function of local concentration. μ^{SR}_{bulk} increased monotonically with decreasing c_{bulk}. The

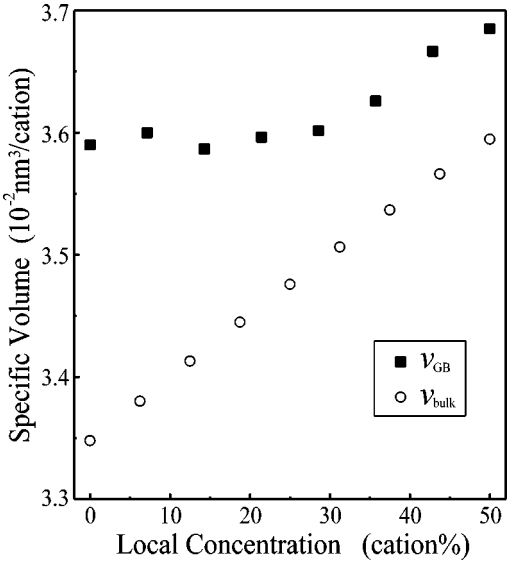

FIG. 7. Specific volumes in the GB and bulk regions as a function of local concentration. Open circles and filled squares are for the bulk and GB regions, respectively.

changes in μ_{bulk}^{C} and μ_{bulk}^{SR} cancel each other out, so that μ_{bulk} showed very little change. In contrast, μ_{GB}^{SR} varied in a similar manner to c_{GB} for $c_{GB} > 28.6$ cation %. However, for $c_{GB} \leqslant 28.6$ cation %, it remained almost independent of c_{GB} and, as a result, μ_{GB}^{SR} was smaller than μ_{bulk}^{SR} for $c_{GB} \leqslant 28.6$ cation %. The smaller μ_{GB} for $c_{GB} \leqslant 28.6$ cation % therefore can be ascribed to the more-or-less constant μ_{GB}^{SR}. The increase in μ_{GB} is also a consequence of the small μ_{GB}^{SR}, as it is dominated by the increase of μ_{GB}^{C}. As mentioned in the previous section, the short-range component of the energy is strongly correlated with the local strain introduced by dopants. These results indicate that local strain in the GB region is relieved in a different manner from in the bulk, especially for $c_{GB} \leqslant 28.6$ cation %.

When a Y^{3+} ion substitutes for a Zr^{4+} ion, the Y^{3+} ion pushes surrounding ions outward due to its larger ionic radius.[50] Consequently, the lattice constants increase. They remain smaller, however, than those for Y_2O_3, which means that there is still local strain around the Y^{3+} ion. This indicates that the local strain is related to changes in volume and that volume change is a good indicator of the local strain introduced by Y^{3+} addition. In order to understand the local concentration dependence of the local strain through volume change, specific volumes were analyzed. The specific volume v was calculated by

$$v = \frac{V}{n_{cat}}, \tag{14}$$

where V is the volume of the GB or the bulk region and n_{cat} is the number of cations in the corresponding region.

Figure 7 shows the specific volumes in the GB region v_{GB} and the bulk region v_{bulk} as a function of local concentration. v_{bulk} increased monotonically with increasing c_{bulk}. v_{GB} also increased with increasing c_{GB} for $c_{GB} > 28.6$ cation %. These changes correspond to the decrease of μ_{bulk}^{SR} and μ_{GB}^{SR}, which implies that relief of the local strain accompanies volume expansion. However, for $c_{GB} \leqslant 28.6$ cation %, v_{GB} remains almost unchanged, just like μ_{GB}^{SR}. This can be interpreted as follows: due to the structural mismatch between two grains, the crystal lattice in the GB region is subjected to a large stress in order for it to accommodate the structural discontinuity and, as a result, the lattice expands. In fact, v_{GB} is larger than v_{bulk} for any local concentration. Since the local space around Zr^{4+} sites in the vicinity of the GB is larger, Y^{3+} ions easily fit into the sites without need for any accompanying volume expansion. Thus, the irregular coordination environments at Zr^{4+} sites in the vicinity of the GB are responsible for smaller μ_{GB}^{SR} and, in turn, μ_{GB}. Y^{3+} addition is not accompanied by volume expansion until c_{GB} reaches 28.6 cation %. Thus, μ_{GB}^{SR} is almost unchanged at this range of concentration, and μ_{GB} increases, as a result of the increase in μ_{GB}^{C}. When c_{GB} reaches 28.6 cation %, almost all the available irregular sites are occupied by Y^{3+} ions, and further Y^{3+} substitution in the GB region is accompanied by volume expansion, which results in a decrease in μ_{GB}^{SR}. Although we have not considered in this section the roles of O^{2-} vacancies in determining the local concentration, the effect of O^{2-} vacancies described in the previous section is not expected to change with increasing concentration.

The segregation of neutrally charged impurities in metals or metalloids occurs to relieve local strain at GBs more than in the grain interior.[51–55] Isovalent dopants in oxides also segregate to GBs in a similar manner.[56,57] In these cases, the segregation is solely determined by atom size mismatch. In contrast, segregation in oxides with aliovalent dopants, such as occurs in YSZ, is controlled not only by the size mismatch (as manifested in the short-range interaction) but also by the Coulombic repulsion between the GB and dopants. This explains the different segregation behavior in oxides with aliovalent dopants compared to that in metals or metalloids, as evidenced by a comparison of segregation at Σ3 (111)/[110] symmetric tilt GBs of fcc metals[54,55] and YSZ, which has been discussed by Shibata *et al.*[27] The results obtained in this study imply that, when foreign cations having different ionic radii and/or different charges are introduced, segregation of a cationic species and its associated defects is different from that of the Y^{3+} ion. In these cases, the local concentration of the segregants will be determined by a different combination of Coulombic and short-range interactions, although they can be analyzed in the same manner as used for Y^{3+} in Fig. 5.

C. Monte Carlo simulation

The results of Sec. III A revealed that the local strain relief is one component of the driving force for segregation, while Coulombic repulsion between the GB and dopants works against the segregation. Chemical potentials were calculated from atomistic simulations in Sec. III B and the results showed that the local concentration of Y^{3+} ions in the vicinity of the GB depends on the chemical potentials in the GB and bulk regions. However, the former analysis was only valid for the dilute limit since it neglected the interaction between pairs of dopants. Although the interactions within the GB or bulk region were taken into account in the latter

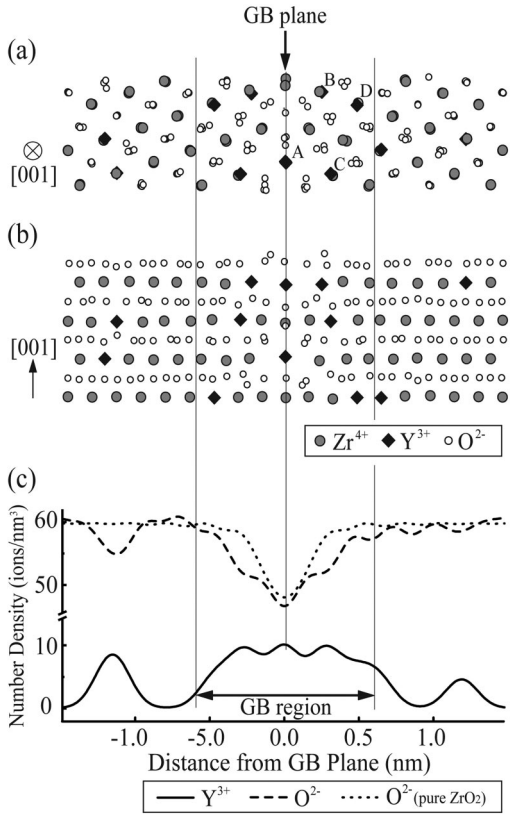

FIG. 8. A typical atomic configuration in the vicinity of a GB projected onto two planes: (a) parallel to [001], and (b) perpendicular to [001]. The supercell contains 24 Y'_{Zr} and 12 $V_O^{\bullet\bullet}$ (15.4 cation % Y^{3+}). (c) shows the distribution of Y^{3+} and O^{2-} ions convoluted by a Gaussian function with FWHM of 0.25 nm. For comparison, the distribution of O^{2-} ions in pure ZrO_2 is also shown.

analysis, the interactions across the regions were neglected. Furthermore, Y'_{Zr} and $V_O^{\bullet\bullet}$ were not allowed to migrate across the regions to decrease energy in the latter analysis. To verify the validity of the results in the preceding sections, a phenomenological simulation without these restrictions was carried out by the Monte Carlo method.

The same simulation cell as that used in Sec. III A was employed, and Y'_{Zr} and $V_O^{\bullet\bullet}$ contents in the cell were varied; the number of Y'_{Zr} and $V_O^{\bullet\bullet}$ were $8n$ and $4n$, respectively, where n was an integer ranging from 1 to 7. In the initial configuration, each ion or vacancy was randomly substituted respectively for one of 156 Zr^{4+} ions and 312 O^{2-} ions in the GB model. The configuration was then optimized until the lattice energy reached a local minimum, as described in Sec. II B.

Figures 8(a) and 8(b) show schematic diagrams of a typical atomic configuration in the vicinity of the GB when the cell contains 24 Y'_{Zr} and 12 $V_O^{\bullet\bullet}$ (total Y^{3+} concentration of 15.4 cation %). At this concentration, not all Y'_{Zr} and $V_O^{\bullet\bullet}$ migrated to the GBs; 16 Y'_{Zr} and 8 $V_O^{\bullet\bullet}$ segregated to the GB regions, and 8 Y'_{Zr} and 4 $V_O^{\bullet\bullet}$ remained in the bulk region. This agrees well with the concentrations predicted based on the chemical potentials in Sec. III B. Y^{3+} ions occupied the Zr^{4+} sites labeled A to D in the figure. These Zr^{4+} sites correspond to the lower energy sites found in Sec. III A (see

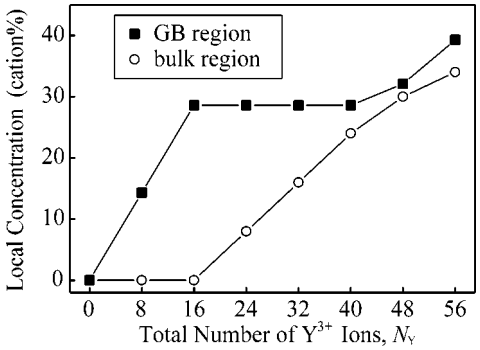

FIG. 9. Local concentrations of Y^{3+} ions obtained by Monte Carlo simulations. Filled squares and open circles show local concentrations in the GB and bulk regions, respectively.

Fig. 3). This indicates that Y^{3+} ions occupy Zr^{4+} sites with irregular coordination environments even when the local Y^{3+} concentration is increased. Distributions of Y^{3+} and O^{2-} ions convoluted by a Gaussian function with a full width at half maximum (FWHM) of 0.25 nm are shown in Fig. 7(c). It is found that O^{2-} ions are deficient in the GB region, and thus O^{2-} vacancies are enriched together with Y^{3+} ions due to cosegregation. It should be noted that the distribution of excess O^{2-} vacancies does not perfectly match that of the Y^{3+} ions; the number of O^{2-} ions on the GB plane is almost the same as that in pure ZrO_2 while Y^{3+} ions are enriched on the plane. Instead, O^{2-} vacancies are enriched 0.2–0.6 nm from the GB plane. This may be perhaps related to the roles of O^{2-} vacancies discussed in Sec. III A. It is speculated that, since the intrinsic O^{2-} vacancies due to the structural discontinuity are present near the GB plane even in pure ZrO_2, the extrinsic O^{2-} vacancies due to Y_2O_3 addition are not needed at the GB core to stabilize the enrichment of Y^{3+} ions. The difference in dopant distributions would create a dipole layer on the GB plane.

Figure 9 shows local concentrations of Y^{3+} ions in the GB and bulk regions as a function of the total number of Y^{3+} ions in the cell N_Y. For $N_Y \leqslant 16$, all of the Y^{3+} ions segregated to the GB regions and the local concentration in the GB regions increased linearly with increasing N_Y (the concentration was identical at both GBs). The local concentration in the GB regions reached 28.6 cation % at $N_Y = 16$ and remained at 28.6 cation % for $16 < N_Y \leqslant 40$. In contrast, the local concentration in the bulk region remained 0 cation % for $N_Y \leqslant 16$ and it increased linearly with increasing N_Y for $N_Y > 16$. These results show that Y'_{Zr} and $V_O^{\bullet\bullet}$ preferentially segregate to the GB regions until the local concentration in the GB regions reaches 28.6 cation %. They start to settle in the bulk region when the local concentration in the GB regions exceeds 28.6 cation %. Changes in the local concentrations both in the GB and bulk regions are in good agreement with those predicted in Sec. III B, and also with experiment.

The above results indicate that increasing concentration does not affect the findings of Sec. III A and that interaction and migration across the regions does not affect the findings of Sec. III B. Consequently, it is concluded that the atomistic mechanisms for segregation revealed in the preceding sec-

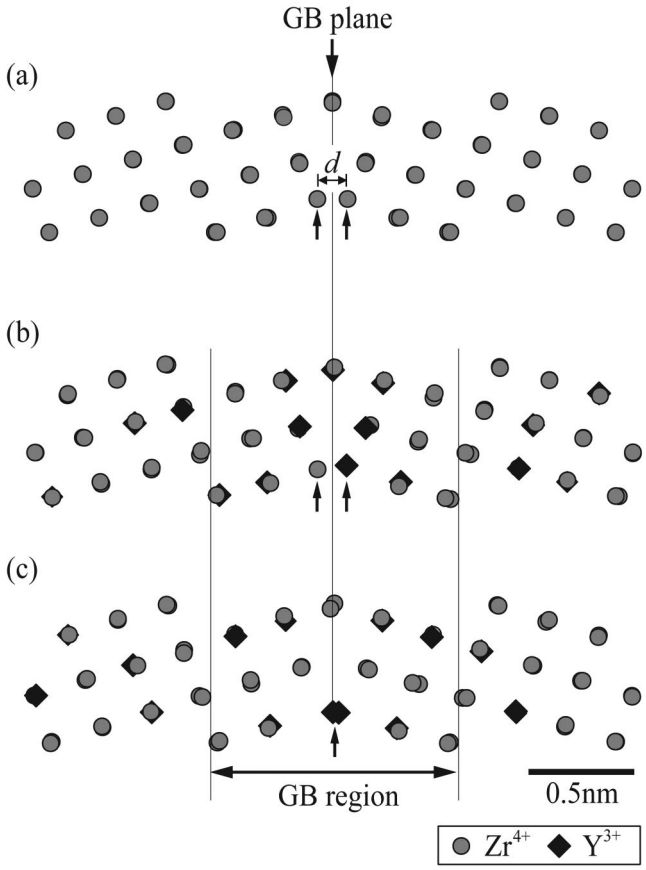

FIG. 10. Comparison of cation configurations in the vicinity of a GB: (a) pure ZrO_2, (b) YSZ with random distribution of Y^{3+} ions, and (c) YSZ with segregation of Y^{3+} ions. In both (b) and (c), the total Y^{3+} concentration is 20.5 cation % and the local Y^{3+} concentration in the GB region is 28.6 cation %.

tions are valid for a wide range of concentrations, and they can thus be used to predict the spatial distribution of Y^{3+} ions and O^{2-} vacancies and their local concentrations in the vicinity of a GB. Although changes in chemical bonding upon mixing have not been taken into account in the potential model used in this study, the agreement with experiment implies that the main component of the driving force for segregation in YSZ can be described by classical interactions.

D. Segregation-induced modification of GB structure

As mentioned earlier, local strain relief is responsible for the GB segregation of Y^{3+} ions and O^{2-} vacancies in YSZ. This implies that GB structures in YSZ may be altered by dopant segregation. It is known in the case of metals that GB core structures and faceting are altered by segregation.[34,58–63] Although no significant change in GB structure is expected in the case of YSZ since ZrO_2, Y_2O_3, and their solid solutions have similar structures, exact understanding of the structure is needed to interpret electron microscope images or to model grain boundary in atomistic simulations. In this section, we examine the effect of segregation on the GB structure in YSZ.

Figure 10(a) shows a schematic diagram of the cation

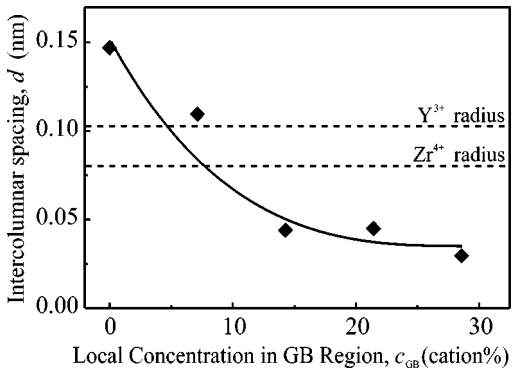

FIG. 11. Intercolumnar spacing in the segregation model illustrated in Fig. 9 as a function of local Y^{3+} concentration in the GB region.

configuration in the vicinity of a Σ5 (310)/[001] symmetric tilt GB in pure ZrO_2, viewed along [001]. Arrows in Fig. 10(a) show two columns of cations that extend along the [001] direction and are separated from the GB plane. The distance between the columns was around 0.15 nm. Since the ionic radius of Zr^{4+} ion is 0.084 nm,[50] occupying all the sites in these columns is energetically expensive; they are only half filled, with the cations aligned in a zigzag manner along the GB plane as shown in Fig. 2.[16,38] Figures 10(b) and 10(c) show schematic diagrams of cation configurations with randomly distributed and segregated Y^{3+} ions, respectively, in YSZ. The total Y^{3+} concentration is 20.5 cation % and the local concentration in the GB region is 28.6 cation % for both cases. When dopants were randomly distributed throughout the cell, the columns at the GB appeared to be similar to those in pure ZrO_2, i.e., they were only half filled. However, the two columns merged into one fully filled column when Y^{3+} ions and O^{2-} vacancies segregated to the GB region.

Figure 11 shows intercolumnar spacing d as a function of the local concentration in the GB region c_{GB} for YSZ with segregated Y^{3+} ions. The intercolumnar spacing decreased with increasing c_{GB}. It decreased to around 0.03 nm for $c_{GB} \geqslant 14.3$ cation %, which is much smaller than the ionic radii of Zr^{4+} and Y^{3+}. This result indicates that the half-filled columns form one fully filled column on the GB plane when the local concentration due to the segregation is greater than around 14.3 cation %. Comparison of Figs. 10(b) and 10(c) indicates that, to form the fully filled column at the GB plane for $c_{GB} \geqslant 14.3$ cation %, Y^{3+} ions occupy Zr^{4+} sites with irregular coordination environments in order of increasing energy. Unless these sites are occupied by Y^{3+} ions, the fully filled column is not formed at the GB plane even if the local concentration increases.

Dickey *et al.* have obtained a *Z*-contrast image of a Σ5 GB in 10 mol % (18.2 cation %) Y_2O_3-doped ZrO_2.[29] The *Z*-contrast image agrees well with the cation configuration in YSZ in Fig. 10(c). The fully filled column appeared as one bright spot on the *Z*-contrast image using a probe of 0.13 nm diameter. If the two half-filled columns with $d \sim 0.15$ nm had formed at the GB, they would have been clearly distinguishable as two separate bright spots in the *Z*-contrast image. This suggests that Y^{3+} ions segregated to the GB in this sample.

HREM and *Z*-contrast image simulations have often been performed to analyze GB structures of YSZ based on the cation configuration of pure, cubic ZrO_2. Our results indicate that an incorrect simulation image of a GB is obtained when pure ZrO_2 or YSZ with randomly distributed dopants is used as the simulation model. GB segregation needs to be taken into account to reproduce and analyze the GB structure of YSZ.

IV. CONCLUSIONS

Numerical analyses of solute segregation at a $\Sigma 5$ $(310)/[001]$ symmetric tilt GB in YSZ have led to the following conclusions.

(1) Relief of the local strain enables the increasing Coulombic repulsion to be overcome and is the driving force for GB segregation. This originates from the irregular coordination environments of Zr^{4+} sites in the vicinity of the GB. Cosegregation of O^{2-} vacancies plays important roles in reducing repulsion between dopants and grain boundary and relieving local strain further. The region of segregation is confined to around 0.6 nm either side of the GB plane.

(2) The local concentration of dopants at the GB can be predicted by balancing the chemical potentials calculated on the atomic level. The chemical potential is the sum of Coulombic repulsion between dopants and local strain relief. The strain release term in the GB region is different from that in the bulk in that addition of dopants is not accompanied by volume expansion. The calculated local concentration of Y^{3+} ions in the GB region is 16.7 mol % for 10.3 mol % Y_2O_3-doped ZrO_2, which is in good agreement with experiment.

(3) These predictions are supported by results from Monte Carlo simulations with an unrestricted treatment for Y^{3+} and O^{2-} vacancy configurations, which showed systematic changes in the local concentration at the GB and grain interior.

(4) GB structure is modified in a systematic way by the concentration of segregants. The degree of segregation therefore needs to be taken into account when interpreting HREM or *Z*-contrast images of the GB.

ACKNOWLEDGMENTS

The authors thank Professor Y. Ikuhara at the University of Tokyo for valuable discussions and Dr. C. A. J. Fisher at the University of Surrey for critical reading of the manuscript. T.O. is supported in part by Murata Manufacturing Co., Ltd.

*Email address: yoshiya@jfcc.or.jp

[1] E. D. Hondros and M. P. Seah, Metall. Trans. A **8**, 1363 (1977).
[2] S. Hoffmann, J. Chem. Phys. **84**, 2 (1987).
[3] A. P. Sutton and R. W. Balluffi, *Interfaces in Crystalline Materials*, edited by R. J. Brook *et al.* (Oxford University Press, New York, 1995), Chap. 7.
[4] K. L. Kliewer and J. S. Koehler, Phys. Rev. **140**, A1226 (1965).
[5] J. A. S. Ikeda and Y.-M. Chiang, J. Am. Ceram. Soc. **76**, 2437 (1993).
[6] X. Guo, Solid State Ionics **81**, 235 (1995).
[7] T. H. Etsell and S. N. Flengas, Chem. Rev. (Washington, D.C.) **70**, 339 (1970).
[8] N. Q. Minh, J. Am. Ceram. Soc. **76**, 563 (1993).
[9] W. J. Fleming, J. Electrochem. Soc. **124**, 21 (1977).
[10] Y. Arachi, H. Sasaki, O. Yamamoto, Y. Takeda, and N. Imanishai, Solid State Ionics **121**, 133 (1999).
[11] J. A. Kilner and R. J. Brook, Solid State Ionics **6**, 237 (1982).
[12] M. J. Verkerk, B. J. Middelhuis, and A. J. Burggraaf, Solid State Ionics **6**, 159 (1982).
[13] S. P. S. Badwal, Solid State Ionics **76**, 67 (1995).
[14] M. Aoki, Y. Chiang, I. Kosacki, L. J. Lee, H. Tuller, and Y. Liu, J. Am. Ceram. Soc. **79**, 1169 (1996).
[15] C. Tian and S.-W. Chan, Solid State Ionics **134**, 89 (2000).
[16] C. A. J. Fisher and H. Matsubara, Solid State Ionics **113-115**, 311 (1998).
[17] F. Wakai, S. Sakaguchi, and Y. Matsuno, Adv. Ceram. Mater. **1**, 259 (1986).
[18] A. H. Chokshi, Mater. Sci. Eng., A **166**, 119 (1993).
[19] T. Sakuma, Mater. Sci. Forum **304-306**, 3 (1999).
[20] Y. Maehara and T. G. Langdon, J. Mater. Sci. **25**, 2275 (1990).
[21] A. Domínguez-Rodríguez, D. Gómez-García, C. Lorenzo-Marín, and A. Muñoz-Berbané, J. Eur. Ceram. Soc. **23**, 2969 (2003).
[22] K. Nakatani, H. Nagayama, H. Yoshida, T. Yamamoto, and T. Sakuma, Scr. Mater. **49**, 791 (2003).
[23] D. Gómez-García, C. Lorenzo-Marín, A. Muñoz-Berbané, and A. Domínguez-Rodríguez, Philos. Mag. **83**, 93 (2003).
[24] N. Shibata, T. Yamamoto, Y. Ikuhara, and T. Sakuma, J. Electron Microsc. **50**, 429 (2001).
[25] N. Shibata, F. Oba, T. Yamamoto, T. Sakuma, and Y. Ikuhara, Philos. Mag. **83**, 2221 (2003).
[26] Y. Ikuhara, P. Thavorniti, and T. Sakuma, Acta Mater. **45**, 5275 (1997).
[27] N. Shibata, F. Oba, T. Yamamoto, Y. Ikuhara, and T. Sakuma, Philos. Mag. Lett. **82**, 393 (2002).
[28] N. Shibata, F. Oba, T. Yamamoto, and Y. Ikuhara, Philos. Mag. **84**, 2381 (2004).
[29] E. C. Dickey, X. Fan, and S. J. Pennycook, J. Am. Ceram. Soc. **84**, 1361 (2001).
[30] Y. Lei, Y. Ito, N. D. Browning, and T. J. Mazanec, J. Am. Ceram. Soc. **85**, 2359 (2002).
[31] N. Shibata, F. Oba, T. Yamamoto, Y. Ikuhara, and T. Sakuma (unpublished).
[32] D. N. Seidman, Mater. Sci. Eng., A **137**, 57 (1991).
[33] T. Watanabe, J. Phys. (France) **46**, C4-555 (1985).
[34] M. Hashimoto, Y. Ishida, R. Yamamoto, and M. Doyama, Acta Metall. **32**, 1 (1984).
[35] M. J. Weins and J. J. Weins, J. Phys. (France) **36**, C4-81 (1975).
[36] R. D. Bourquin, *Computer Simulation for Materials Applications*, edited by R. J. Arsenault, J. R. Beeler, Jr., and J. A. Simmons, Nucl. Metall. **20**, 325 (1976).

[37] N. Sawaguchi and M. Okazaki (unpublished).
[38] Z. Mao, S. B. Sinnot, and E. C. Dickey, J. Am. Ceram. Soc. **85**, 1594 (2002).
[39] P. P. Ewald, Ann. Phys. **64**, 253 (1921).
[40] L. Minervini, M. O. Zacate, and R. W. Grimes, Solid State Ionics **116**, 339 (1999).
[41] L. Minervini, R. W. Grimes, and K. E. Sickafus, J. Am. Ceram. Soc. **83**, 1873 (2000).
[42] M. O. Zacate, L. Minervini, D. J. Bradfield, R. W. Grimes, and K. E. Sickafus, Solid State Ionics **128**, 243 (2000).
[43] J. D. Gale, J. Chem. Soc., Faraday Trans. **93**, 629 (1997).
[44] M. L. Kronberg and F. H. Wilson, Trans. AIME **185**, 501 (1949).
[45] N. Metropolis, A. W. Rosenbluth, M. N. Rosenbluth, A. H. Teller, and E. Teller, J. Chem. Phys. **21**, 1087 (1953).
[46] A. P. Sutton and V. Vitek, Acta Metall. **30**, 2011 (1982).
[47] W. D. Kingery, J. Am. Ceram. Soc. **57**, 74 (1974).
[48] P. Li, I.-W. Chen, and J. E. Penner-Hahn, Phys. Rev. B **48**, 10 063 (1993); **48**, 10 074 (1993); **48**, 10 082 (1993).
[49] N. Ma, S. A. Dregia, and Y. Wang, Acta Mater. **51**, 3687 (2003).
[50] R. D. Shannon and C. T. Prewitt, Acta Crystallogr., Sect. B: Struct. Crystallogr. Cryst. Chem. **25**, 925 (1969).
[51] A. Maiti, M. F. Chisholm, S. J. Pennycook, and S. T. Pantelides, Phys. Rev. Lett. **77**, 1306 (1996).
[52] W. T. Geng, A. J. Freeman, G. B. Olson, and R. Wu, Phys. Rev. B **62**, 6208 (2000).
[53] R. Besson, A. Legris, and J. Morillo, Phys. Rev. B **64**, 174105 (2001).
[54] J. D. Rittner and D. N. Seidman, Acta Mater. **45**, 3191 (1997); Phys. Rev. B **54**, 6999 (1996).
[55] M. Yan, M. Šob, D. E. Luzzi, V. Vitek, G. J. Ackland, M. Methfessel, and C. O. Rodriguez, Phys. Rev. B **47**, 5571 (1993).
[56] D. M. Duffy and P. W. Tasker, Philos. Mag. A **50**, 155 (1984).
[57] H. S. Domingos and P. D. Bristowe, Scr. Mater. **41**, 1347 (1999).
[58] M. Guttmann, Metall. Trans. A **8**, 1383 (1977).
[59] C. Pichard, M. Guttmann, J. Rieu, and C. Goux, J. Phys. (Paris) **36**, C4-151 (1975).
[60] J. R. Rellickm, C. J. McMahon, Jr., H. L. Marcus, and P. W. Palmberg, Metall. Trans. **2**, 1492 (1971).
[61] C. Pichard, J. Rieu, and C. Goux, Mem. Sci. Rev. Metall. **70**, 13 (1973).
[62] A. Donald, Philos. Mag. **34**, 1185 (1976).
[63] G. H. Bishop, W. H. Hartt, and G. A. Bruggeman, Acta Metall. **19**, 37 (1971).